Int J Adv Manuf Technol (2013) 68:1479–1490
DOI 10.1007/s00170-013-4936-7

ORIGINAL ARTICLE

Interfacial characterization of T3 copper/35CrMnSi steel dissimilar metal joints by inertia radial friction welding

Ying Wang · Jian Luo · Xiaoming Wang · Xiaoling Xu

Received: 9 August 2011 / Accepted: 21 March 2013 / Published online: 21 April 2013

Abstract This paper reports our work on developing an inertia radial friction welding (IRFW) technique to join a 35CrMnSi steel shaft with a T3 copper (Cu) annular block. The microstructure of the T3 Cu/35CrMnSi steel dissimilar metal joint materials is studied. The results show that a quenching zone exists obviously near the interface on the 35CrMnSi steel side, and a soft region exists in the heat-affected zone (HAZ) on the 35CrMnSi steel side also according to microhardness measurements. The super-plastic deformation zone (SDZ) is more obvious on the T3 Cu side than on the 35CrMnSi steel side. The microhardness of the SDZ is higher than that of the T3 Cu base metal on the T3 Cu side. Element diffusion occurs through both sides of the dissimilar metal welded joint. The hardening phenomenon existing in the joint is attributed to the effect of the plastic deformation, element diffusion, and recrystallization. New $FeCu_4$ and Cu_9Si compounds are formed in the friction bonding interface, which suggests that the T3 Cu and 35CrMoSi steel dissimilar metals experience a landmark metallurgical bonding. The shear strength test results show that the T3/35CrMnSi dissimilar metals are joined together successfully in the IRFW process.

Keywords Interface features · Inertia radial friction welding · Dissimilar joint · Element diffusion

Y. Wang · J. Luo (✉) · X. Wang
State Key Laboratory of Mechanical Transmission, Chongqing University, Chongqing 400030, China
e-mail: luojian2007@gmail.com

X. Xu
Chongqing Honglingxiang Mechanical Development Co. LTD, Chongqing 401120, China

1 Introduction

Combinations of dissimilar materials have found increasingly wide industrial applications due to their microstructural advantages over single metals, such as in aerospace, petroleum, aviation, shipbuilding, railway, power generation, and petrochemical industry [1, 2]. Dissimilar metal offers the potential to utilize the advantages of different materials often providing unique solutions to engineering requirements. These advantages include not only the material properties advantages, but also technical advantages and the benefit in terms of production economics, such as desired product properties and low cost [3, 4]. So the dissimilar metal joints are widely used in engineering structures, owing to these attributes of good mechanical properties (like stiffness) of one material and either high electrical conductivity or low specific weight of second material [5, 6]. Many situations arise in industrial practices which call for joining of dissimilar materials. Consequently, welding and joining techniques for dissimilar materials have received considerable attention and are becoming increasingly important in the recent years [7].

At nuclear power generation industries, one of the applications of dissimilar metals welding joints are employed to connect copper (Cu) and low alloy steel. In considering structural joints between Cu and steel, weldability problems should be taken into account firstly, the welding of general metals or alloys is an experienced topic, but the dissimilar welding represents a major scientific and technical procedures difficult [8], especially good bonding between Cu and steel is challenged due to significant differences in the physical, chemical, thermomechanical and metallurgical properties of the based metals to be joined, such as expansion coefficient, conductivity, and specific heat for thermal properties differences [9].

Research conducted on the welding of Cu to steel ranges from fusion welding to solid-state welding processes [5, 10, 11], specific processes investigated include as arc fusion welding, electromagnetic hybrid arc welding, laser welding, and so on [12–17]. One of the most critical problems associated with joining dissimilar materials is the formation of residual stresses on fusion welding process, which can be measured experimentally by using a new hole-drilling method accurately [18]. On the other hand, fusion welding joints are faced with the problem of coarse grains in the weld transition zone or heat-affected zone (HAZ) and consequent low toughness and ductility, the conventional arc welding technique is unsuitable for joining dissimilar metal, it is difficult to achieve defect-free Cu and steel dissimilar joints using the conventional fusion methods [19–22]. Hence, it is important to develop solid-state welding technology to join Cu and steel dissimilar materials. The use of solid-state welding technique generally is associated with reduced formation of some defect or weak microstructure. Friction welding is one of the advanced techniques of solid-state joining, which allows joining at relatively low temperatures with an overall short thermal cycle, although under some high friction, the interfacial temperature may reach the melting point of the material [23–26].

The inertia radial friction welding (IRFW) is a special technique which is applied in joining the dissimilar metal materials [27]. The IRFW technique is unlike standard the axial friction welding in that it offers the many advantages [28]. IRFW is a one-shot welding process with great potential to join Cu and steel [29]. In the past decades, many researchers have developed the IRFW process for T3 Cu/35CrMnSi steel dissimilar materials. Nonetheless, the IRFW for Cu and low alloy steels dissimilar metal joining also remains large challenging. No further information pertaining to the level of plastic deformation and element distribution imposed at the interface of the T3 Cu/35CrMnSi steel welded joint in IRFW is available. And the detailed research works in relation to interfacial characteristics of the IRFW Cu and steel dissimilar joints were relatively few and uncompleted specially. So our present study aims to produce T3 Cu and 35CrMnSi dissimilar metal joints by IRFW, and then to investigate the effects of plastic deformation, element distribution, microhardness on the mechanical strength of the resulting microstructures, and interfacial characteristics both analytically and experimentally, such as an optical microscope (OM), a scanning electron microscope (SEM), and the energy dispersive system (EDS). Many experiments are conducted to test a T3 Cu annular block welding around a 35CrMnSi steel shaft with different IRFW parameters. The characterization of interface in the radial direction, which plays a key role of T3 Cu/35CrMnSi dissimilar metal welded joints, will be analyzed. The relationships between microstructure and interface bonding properties have been comprehensively studied with different welding formations and technologies. A new model is issued completely to explain the formation mechanism of T3 Cu/35CrMnSi dissimilar metal joint on the IRFW process. These research results will provide a guide or implement of solid phase welding technique for many dissimilar metals joining.

2 Materials and experiments

2.1 Materials and work pieces

In this study, the T3 Cu annular block is a 99.9 % pure Cu. The chemical composition of the 35CrMnSi steel is shown in Table 1.

The T3 Cu annular block has an inner diameter of 32.4 mm, outer diameter of 50.1 mm, and width of 4.5 mm, while the 35CrMnSi steel shaft has a length of 90 mm and diameter of 30 mm (shown in Fig. 1).

2.2 Welding preparation and experimental equipment

Prior to welding, annular blocks were soaked in the mixture of 95 % phosphoric acid and 5 % nitric acid solution for about 15 min in order to remove the surface oxide. They are then rinsed with water and dried finally. The 35CrMnSi steel shafts were, firstly, ground with sand papers until the surface oxide was removed, and cleaned with acetone to remove contamination, if any; they were atmospherically dried. After these preparations, the welding experiments were performed in a CT-25 IRFW machine, or the IRFW machine as shown in Fig. 2.

2.3 Welding process

The schemes of the T3/35CrMoSi IRFW device and welding parameters are shown in Fig. 3.

There is an important the pressure conversion system in this IRFW equipment. It can change the axial thrust force into a radial force by a special bonding mobile fixture with a tapered body. The diagram of the tapered fixture and the radial force on the T3/35CrMoSi work pieces in IRFW are shown in Fig. 4.

The important working process of T3/35CrMoSi dissimilar metal IRFW is described as follows:

Table 1 Chemical composition of 35CrMnSi steel (in weight percent)

Element	C	Si	Mn	Cr	Fe
Content	0.32~0.39	1.10~1.40	0.80~1.10	1.10~1.40	Balance

1. At the beginning of welding, the flywheel and the shaft will be rotated to a certain high speed by the spindle motor to store a predetermined amount of energy. The flywheel is then turned off the spindle motor by a clutch. The tapered mobile fixture changes the axial force into the radial force, and this radial force works on the annular block, the deformation of the T3 Cu annular block takes place gradually.
2. When two work pieces touch each other, the relative frictional motion produces the friction action on the contact interface begins under the pressure of the radial force. The resulting frictional heat raises the temperature of the metal in the contact area quickly until the metal is heated to the plastic state.
3. The axial pressure is strengthened suddenly, which gives the piston a great instantaneous driving force and eventually leads to a sudden increase in the radial force produced by the mobile fixture through the piston. Finally, after a certain time of pressure application, the welding joint is finished and is released from the clamp.

In this experiment, the T3/35CrMoSi IRFW parameters are used in the Table 2.

2.4 Specimen preparation and material charaterization methods

A wire-cut electrodischarge machine was used for metallographic specimen preparation after IRFW. Specimens of transverse and longitudinal cross-sections were made from the interface of a dissimilar metal IRFW joint. The metallographic specimens of longitudinal cross-sections were used for microstructure observations, which were prepared by mechanical polishing with the standard metallographic technical procedure. Because it is from the T3/35CrMoSi IRFW joint, the T3 Cu side was etched with an ammonia solution containing 8 % $CuCl_2$ while the 35CrMoSi steel side is etched by an alcohol solution with 4 % nitric acid, respectively. Then the ultrasonic cleaner is used to clean the metallographic specimens of T3/35CrMoSi IRFW joint.

The OM was used to view the macrostructure of the metallographic specimens, and SEM examines the microstructure

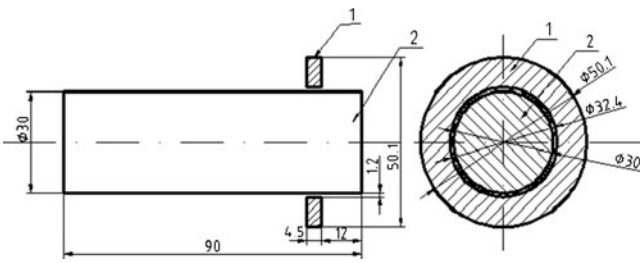

Fig. 1 Dimensions of the T3 Cu annular block and the 35CrMnSi steel shaft (*1*, T3; *2*, 35CrMnSi; in millimeters)

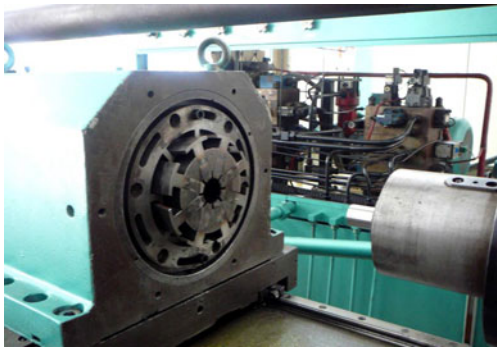

Fig. 2 CT-25 type IRFW machine

characteristics of welding samples. Element distribution analyses were carried out using an EDS, which is a tool attached to the SEM. The X-ray diffraction meter (XRD) was used to investigate and characterize the phase composition of a desired position in the T3/35CrMoSi IRFW joints with a CuKα radiation at 40 kV/150 mA. The Vickers microhardness tester was used for the microhardness measurement under 9.80 N load and 10 s keeping time. The electronic universal machine was used to measure the strengths.

3 Results and analysis

3.1 Macrostructure and microstructure

The macro-morphology of a T3/35CrMoSi IRFW joint is shown in the Fig. 5. The Cu ring surface shows the appearance of the indentation, deformation along the radial and axial directions of the 35CrMnSi steel shaft. The shape of the Cu ring changes form narrow and thickness (size, 4.5× 8.85 mm) to width and thin (size,11.7×1.25 mm) appearance. The Cu ring generates a lot of flashes near the edge of the welding joint. The shape of the 35CrMoSi steel shaft does not show an obvious variation.

Figure 6 shows the microstructure of the based metal of an IRFW joint. Figure 6a shows the microstructure of the 35CrMnSi steel base metal in the quenched state, which consists of the sorbite and the ferrite structures. Figure 6b shows the microstructure of that the 35CrMnSi steel base metal is characterized by the equiaxed ferrite in a uniform distribution state and the sorbite surrounded the ferrite. The average grain size of the 35CrMnSi steel base metal is about 0.17 mm. In Fig. 6c, the base metal of the T3 Cu ring is in a cold drawn state, which is composed of a single α-phase Cu. The average grain size of the base metal of the T3 Cu ring is about 0.08 mm.

Figure 6d shows a typical interface of the T3/35CrMnSi IRFW joint. To a great extent, the bonding strength of the interface is determined by the welding parameters. Particularly, there are three key welding parameters in IRFW, such as the thrust force, rotation speed, and displacement, which

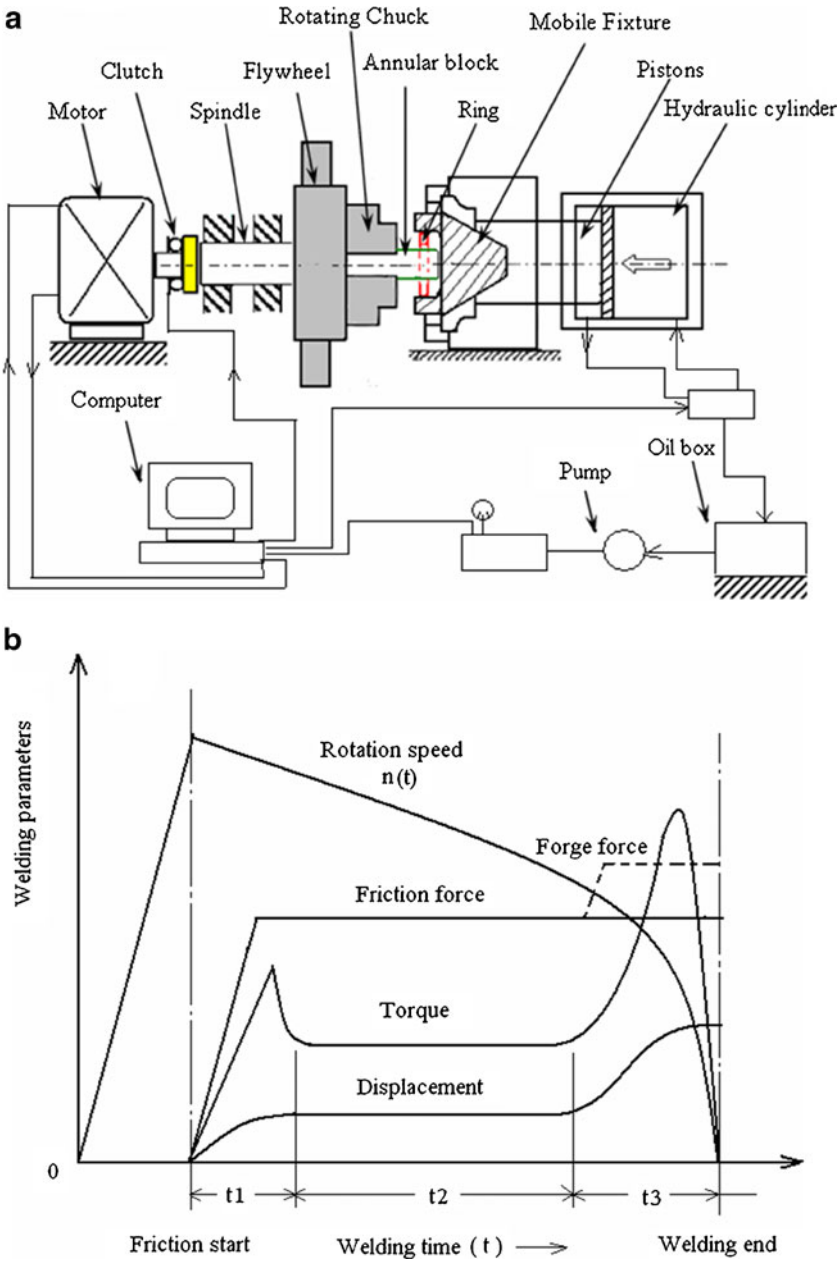

Fig. 3 Schematic of the T3/35CrMoSi IRFW device and welding parameters. **a** IRFW device. **b** Welding parameters

are shown in Fig. 3b. The 35CrMnSi steel shaft with trapezoidal grooved is another typical joining method in order to improve the bonding strength of the T3/35CrMoSi IRFW joint by strong plastic deformation.

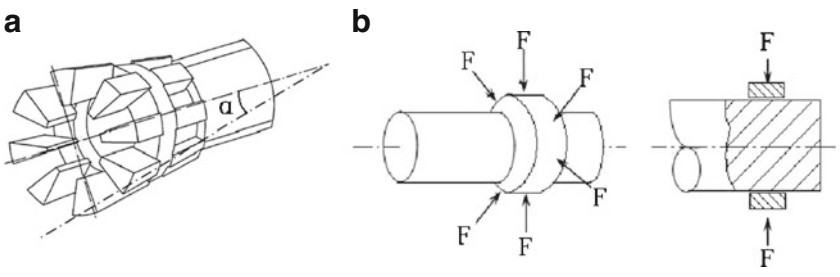

Fig. 4 Diagram of the radial force on the T3/35CrMoSi workpieces. **a** Tapered fixture. **b** Radial force transfer

Table 2 IRFW parameters for T3/35CrMnSi dissimilar metals joint

Variable	Unit	Value
Moment of inertia	kg m^2	0.636
Rotation speed	rpm	3,000
Friction pressure	MPa	78.53
Forge pressure	MPa	178
Welding time	s	9

The panorama microstructure views of the T3/35CrMnSi l IRFW joint is shown in Fig. 7. Figure 7a is a cross-section of the joints. Figure 7b is an optical macrostructure of the interface, which is a locally magnified image for Fig. 7a. Figure 7c is the micrographs of the interface of the joint from Fig. 7b. The T3/35CrMnSi IRFW joint can be divided into four feature zones from the interface to two sides, which are identified as the super-plastic deformation zone (SDZ), the quenching zone (QZ), the HAZ, and the base material (BM) on the T3 Cu side or the 35CrMnSi steel side, respectively. The SDZ lies on the T3 Cu side, as shown in Fig. 7d, because the plastic deformation of T3 Cu is stronger or more obviously than that of 35CrMnSi steel. Both the T3 Cu side and the 35CrMnSi steel side have the HAZ and BM, but the HAZ of the 35CrMnSi steel side is more obvious than that on the T3 Cu side (seen in Fig. 7d, c) because the T3 Cu has a high-thermal conductivity.

The QZ lies on the 35CrMnSi steel side, as shown in Fig. 7e. The microstructure of the QZ on the 35CrMnSi steel side is composed of lath martensite. The HAZ on the 35CrMnSi steel side is shown in Fig. 7f, which can be seen that size of the microstructure in the HAZ is a slightly coarser than that in the QZ on the 35CrMnSi steel side. Figure 7f presents the microstructure of the HAZ, which is also lath martensite on the 35CrMnSi steel side.

Compared with the HAZ of the 35CrMnSi steel side, the BM microstructure of the 35CrMnSi steel is fine in Fig. 6a. It also indicates that the influence of frictional heat on the HAZ is strong and obvious on the 35CrMnSi steel side. However, there is no trace of lath martensite in the BM of the 35CrMnSi steel.

3.2 Interface characteristics

The microstructure of the interface of the T3/35CrMoSi dissimilar metal IRFW joint is shown in Fig. 8. Compared with the BM of T3 Cu in Fig. 6c, Fig. 8a shows a fine grain microstructure of the SDZ on the T3 Cu side obviously. Figure 8b also presents the grain size changes from the HAZ to the BM in T3 Cu. The fine grain of the SDZ can be attributed to the reason that the T3 Cu annular block, firstly, is subjected to a comparable IRFW thermal cycle and then a strong forging force. Because the T3 Cu has a good plastic property, it exhibits super-plastic deformation behaviors around the 35CrMnSi steel shaft in IRFW.

The super-plastic deformation of T3 Cu is close to a state of semi-molten under the influence of frictional heating, which is shown in Fig. 8c. The grain or dendrite of T3 Cu is crushed and rapidly cooled in a short welding time. The grains of the SDZ are refined as a result of the effect of the forging force. We believe that the formation mechanism of the fine grain layer in the SDZ on the T3 Cu side is due to the combined effect of both semi-solid squeezing casting and super-plastic forge deforming, according to the Figs. 7d and 8a, c. Figure 8d shows the microstructure of the QZ on the 35CrMnSi steel side. There is also a refined grain layer in Fig. 8e. In Fig. 7e, the lath martensite can be observed in this zone, as a consequence of the quenching-like heat treatment. Three reasons are explained about the QZ:

1. Influence of a high welding temperature. The welding temperature on the interface of the IRFW joint reaches a high value, near the melting point of T3 Cu metal, so that a phase transfer might have taken place on the 35CrMnSi steel side. Based on the simple iron (Fe)–carbon © binary phase diagram, the phase microstructure (sorbite and ferrite) of the 35CrMnSi steel BM should have changed into austenite (interstitial solid solution of C in γ-Fe) during IRFW process since their temperature reaches austenitizing range due to the frictional heat.
2. Thermal physical properties of T3 Cu and 35CrMnSi steel. T3 Cu has an excellent thermal conductivity property, but 35CrMnSi has a low-thermal conductivity but a

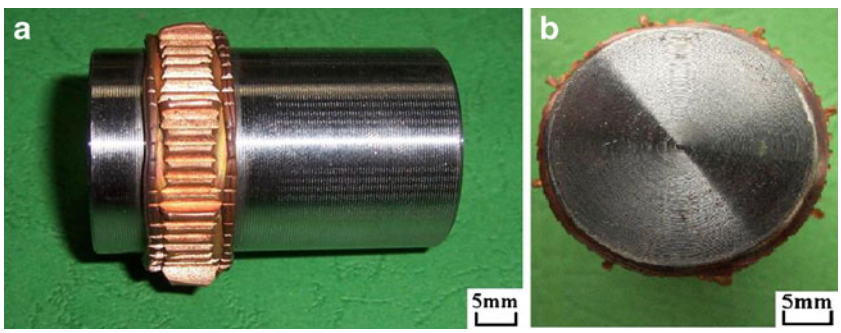

Fig. 5 The macro-morphology of a T3/35CrMoSi dissimilar metal IRFW joint. **a** Appearance. **b** Left view

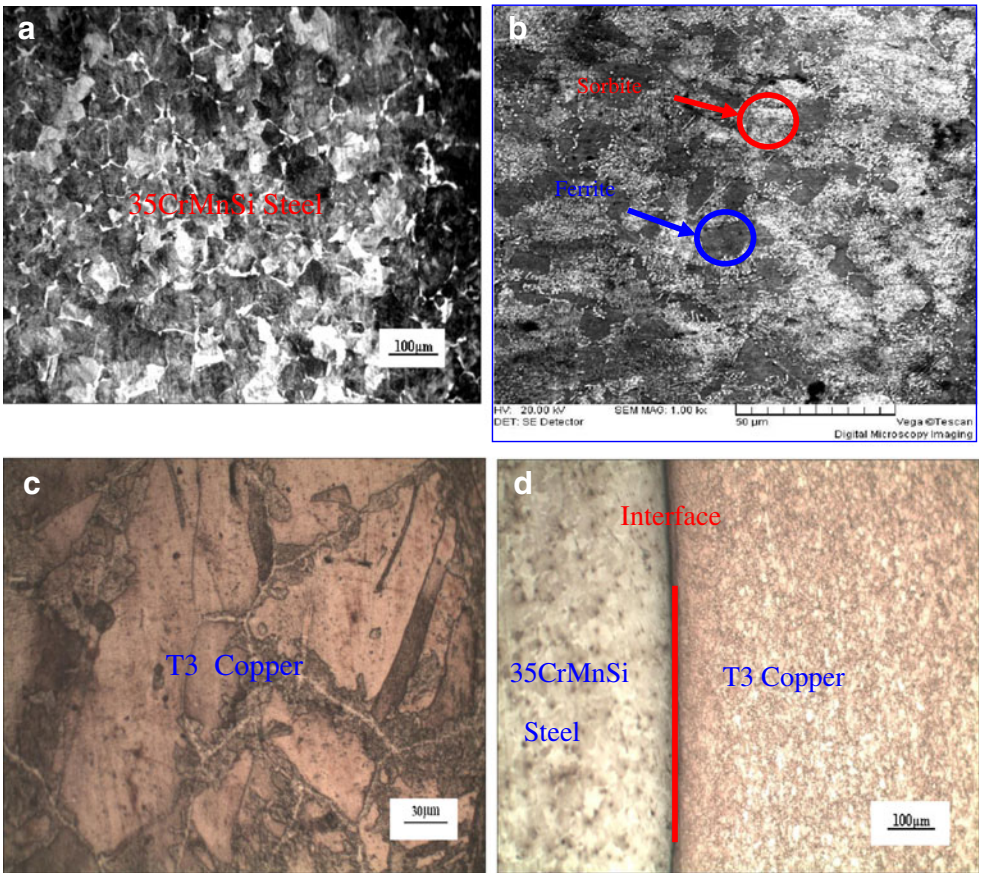

Fig. 6 Microstructure of the base metal of a T3/ 35CrMnSi dissimilar metal IRFW joint

high linear thermal expansion coeffient; therefore, heat transfer of T3 Cu is faster than that of 35CrMnSi steel. Moreover, the BM temperature of T3 Cu is the room temperature, which is far away from the interface of the IRFW joint. The detail is shown in Section 3.5.

3. Characteristic of IRFW. Because the welding speed of IRFW is quick and the welding time is short (less than 1 s), the welding continuous cooling transformation speed is very fast. The temperature gradient of the 35CrMnSi steel near the interface of the IRFW joint is large. Moreover, due to the friction force and the forge force, both the plastic deformation and thermal expansion of the 35CrMnSi steel are also very strong. Therefore, the high temperature austenite of 35CrMnSi welding seam could be rapidly cooled in IRFW. When the cooling rate is the same as the critical quenching rate in a short welding time, some solid solution of C in the austenite has no time to precipitate; as a result, the martensite (supersaturated solid solution of C in α-Fe) is formed on the 35CrMnSi steel side near the interface of the IRFW joint. A very obvious bright white band of the QZ can be observed on the 35CrMnSi steel side near the interface, which shown in Fig. 8d.

Figure 8g shows the interface of the IRFW joint with a trapezoidal groove. When there has a trapezoidal groove in the 35CrMnSi side, T3 Cu produces plastic deformation following the bottom of groove, and then the groove is filled with the plastically deformed T3 Cu. The bonding strength of T3/35CrMoSi dissimilar metal IRFW joint is better because there is a stronger plastic deformation, and further details will be discussed in the future.

3.3 Element diffusion in the interface

Element diffusion can be detected from the chemical characterization of the interface region of T3/35CrMoSi dissimilar metal IRFW joint. The SEM images with EDS analyses of an interface cross section are shown in Fig. 9. In Fig. 9a, b, the interface metal flowing on the 35CrMnSi steel side and SDZ on the T3 Cu side can also be clearly observed. In addition, Fig. 9a displays the EDS scans for Cu, Fe, oxygen (O), and C. Figure 9c, d show the EDS point analysis results, respectively corresponding to spectrums 1 and 2 in the Fig. 9b. The distributions of Cu and Fe element in the bonding interface of the joint are plotted in Fig. 10, separately.

The EDS results presented in Figs. 9 and 10 show that Fe distribution decreases suddenly in the interface from the 35CrMnSi steel side to the T3 Cu side. (Note: EDX cannot tell the chemical state, therefore, the signal can only indicate Fe, not the pure element, nor the accurate form of a compound). So is the Cu distribution from the cu-rich T3 side to the 35CrMnSi steel side. Nevertheless, it is obviously that

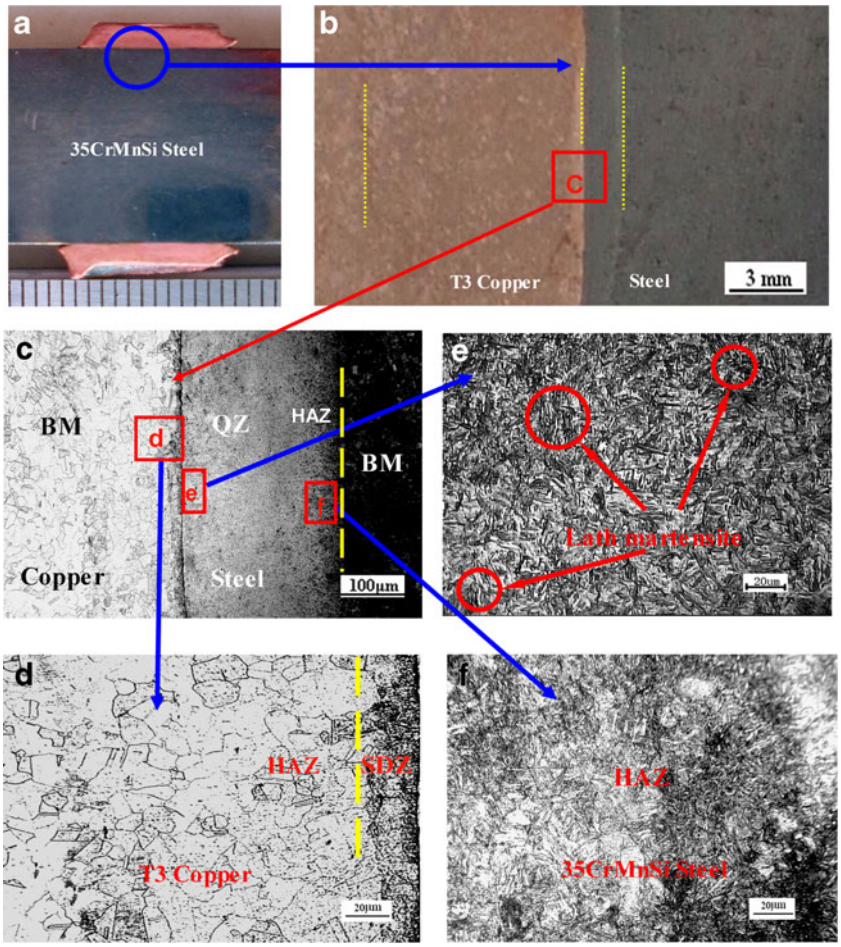

Fig. 7 Microstructure of a T3/35CrMnSi dissimilar metal IRFW joint. **a** Cross-section of the joints. **b** Macrographs of the interface of the joint. **c** Micrographs of the interface of joint. **d** Micrographs of both the HAZ and SDZ in T3 Cu. **e** Micrographs of the QZ at the 35CrMnSi steel side. **f** Micrographs of the HAZ at the 35CrMnSi steel side

the content of Cu on the 35CrMnSi steel side is more than content of Fe on the T3 Cu side, apparently the diffusion speed and ability of Cu into 35CrMnSi steel is higher than that of Fe into T3 Cu during the welding process. In the welding interface, the cu content is more than that of Fe in the IRFW joint. The EDS analysis reveals 17.06 wt.% Cu in spectrum 1 and 5.19 wt.% Fe in spectrum 2. Note that spectrums 1 and 2 separately lie in the QZ of the steel side and the SDZ on the Cu side (see Fig. 9(b)), the content of Fe in the SDZ of the T3 Cu side is more than that in the HAZ or the BM separately, Cu element has a similar distribution independently.

These characterized elements of 35CrMnSi steel, such as chromium (Cr), manganese (Mn), and silicon (Si), are not found on the T3 Cu side, as shown in Fig. 9d. The diffusion abilities of these elements in T3 Cu are weak, or the diffusion speed of these elements in T3 Cu is very slow compared with the short welding time. C and O roughly exhibit steady distributions in the IRFW joint without significant fluctuation at both sides of the welding interface. Their contents are so small, especially C, as shown in Fig. 9a, that they are nearly negligible in the T3/35CrMoSi IRFW joint.

The depth of element diffusion is less than 3 μm from the bonding interface. Because the welding time is very short and the welding temperature is less than the melting point of the 35CrMnSi steel, it is difficult for the defused elements to reach a deeper location and accumulate a higher concentration. However, although only a thin layer of element diffusion is identified at each side of the T3/35CrMnSi interface, it is important to note that the T3/35CrMoSi joint build a tight bonding.

3.4 XRD analysis

XRD should provide another evidence of element diffusion. Figure 11 shows the XRD analysis of the welding interface of the T3/35CrMoSi IRFW joint, which suggests some new phases formed in the f interface, such as $FeCu_4$ and Cu_9Si intermetallic compounds.

In Fig. 11, the appearances of $FeCu_4$ compound in IRFW joint further confirms the element diffusion on the two sides of work pieces. Because the 35CrMnSi steel has no Cu elements, and the T3 Cu has few Fe elements, seen in Table 1. Even though the diffusion distance of Cu or Fe element is very short, and the content of Cu into the 35CrMnSi steel side, or the content of Fe into the T3 Cu side is not high based on the EDS analysis shown Figs. 9 and 10, the T3/35CrMoSi d IRFW joint is considered a strong bonding as a consequence of the formation of the $FeCu_4$ compound.

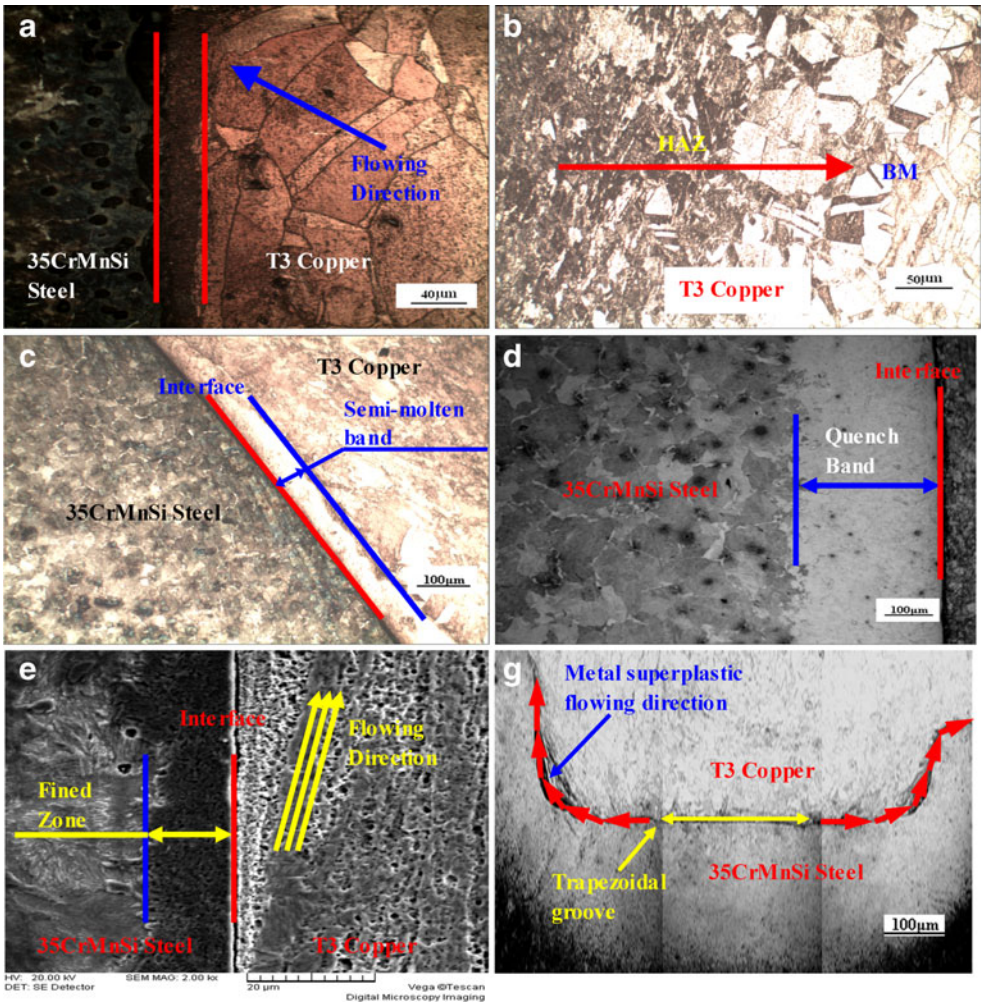

Fig. 8 Interface characteristics of a T3/35CrMnSi dissimilar metal IRFW joint. **a** SDZ at the T3 Cu side. **b** HAZ at the T3 Cu side. **c** Semi-molten state of the T3 Cu side. **d** White bright quench band of the 35CrMnSi side. **e** Interface micrographs of the IRFW joint. **f** Metal plastic flowing of the IRFW joint with trapezoidal grooves. **g** Friction interface of the IRFW joint with a trapezoidal groove

Because there is no Si element detected on the T3 Cu side of the joint by the EDS analysis (Fig. 9), the Cu_9Si intermetallic compound occurs only on the 35CrMnSi side. When the Cu_9Si intermetallic compound formed in the welding interface, a hardness difference should be deleted because the Cu_9Si intermetallic compound is a hard and brittle phase, which should be harmful to the bonding strength of the welding joint. The content of Cu_9Si intermetallic compound needs to be controlled to a safe level. Crystalline phase $FeCu_4$ is also formed at both sides of the welding interface; this phase also has an obvious effect on the mechanical properties of the welding joint, such as the hardness.

3.5 Interface microhardness

The microhardness variation across the interface of both sides of the T3/35CrMoSi IRFW joint is shown in Fig. 12, which reveals the following.

1. The maximum microhardness value on the T3 Cu side is about 78.2 HV, which lies in the SDZ and near the interface of the welding joint. On the T3 Cu side, the microhardness of the SDZ is higher than that of the materials in other zones. In the SDZ of T3 Cu side, the microhardness increases near the interface. However, there is no obvious hardness variation from the BM to HAZ, and the microharness range is 51.4~61.2 HV, likely due to the fact that the T3 Cu is of an excellent thermal conductor, so the HAZ of T3 Cu side is not very clear than that of 35CrMnSi side. On the other hand, dynamical recrystallization might have taken place in the SDZ in a super-plastic deformation process, so that the grain size in the SDZ is smaller than that in the BM. There is element (Fe or other) diffusion or infiltration in this zone. The formation of the $FeCu_4$ crystalline phase (owing to the element diffusion shown in Figs. 9 and 11) and the refined grain (shown in Figs. 7 and 8) should all contribute to the microhardness of the T3 Cu side in the SDZ. There is no intermetallic compound Cu_9Si in the SDZ of the T3 Cu side. This interpretation is supported by the theories of fine grain strengthening and solid solution strengthening. Both the microstructure and the new phase affect the microhardness of the bonding interface of T3/35CrMoSi joint.

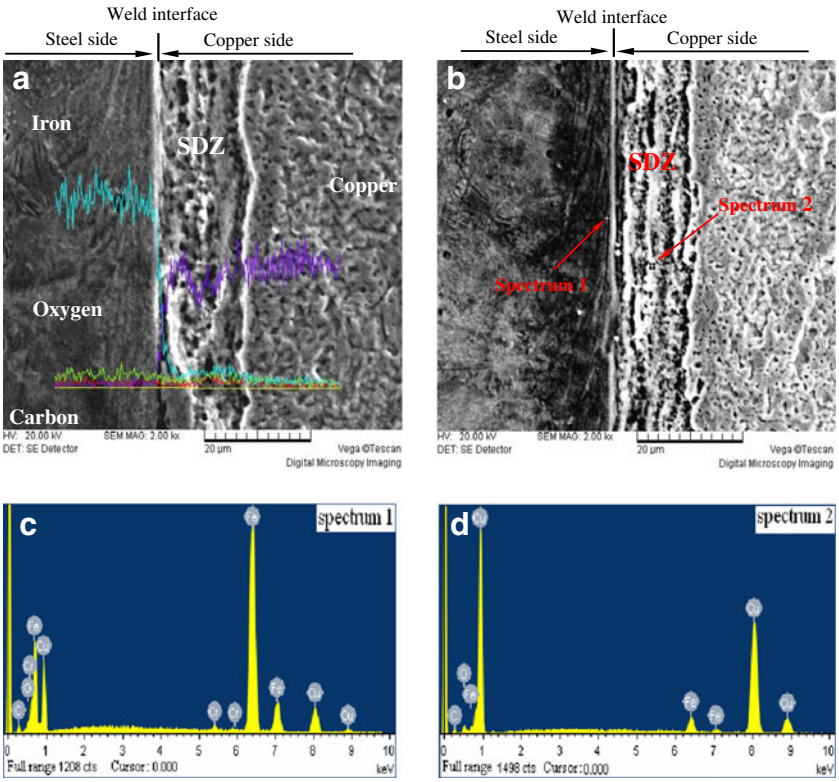

Fig. 9 SEM images and EDS signals for the interface region of the T3/35CrMoSi dissimilar metal IRFW joint: **a** SEM image with EDS signals; **b** SEM image with EDS signals at another location in interface region; **c** EDS spectrum of the gray area in the QZ at the 35CrMnSi steel side, i.e., spectrum 1 in (**b**); **d** EDS spectrum of the white area in the SDZ at the Cu side, i.e., spectrum 2 in (**b**)

2. On the 35CrMnSi steel side, the maximum microhardness value is about 660HV and lies in the QZ of the welding joint, not close to the bonding interface. The distance is about 0.165 mm away from the interface. The minimum hardness value is about 330 HV and lies in the HAZ, which is about 0.526 mm away from the interface. The average microhardness value of QZ is much higher than that of BM; even the microhardness value of BM is higher than that of the HAZ. This interesting phenomenon can be explained by the microstructure and compounds of on the 35CrMnSi steel side shown in the Figs. 7, 8, and 11. On the 35CrMnSi steel side, the high microhardness near the interface indicates an obvious different microstructure from the BM of the 35CrMnSi steel. It confirms that the high microhardness zone is the QZ and the main microstructure in this zone is the quenching martensite phase, because the formation of martensite changes the average microhardness value of the sorbite and ferrite dominant BM. In addition, it is well known that the coarser microstructures of the HAZ on the 35CrMnSi steel side are responsible for the lowest hardness of the sorbite and ferrite phases.

Why does the max peak of microhardness lie in the middle of the QZ, rather than near the interface? Figure 13

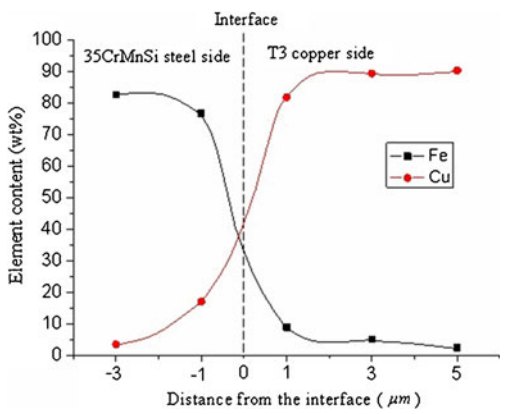

Fig. 10 Fe and Cu diffusion in the bonding interface of the IRFW joint

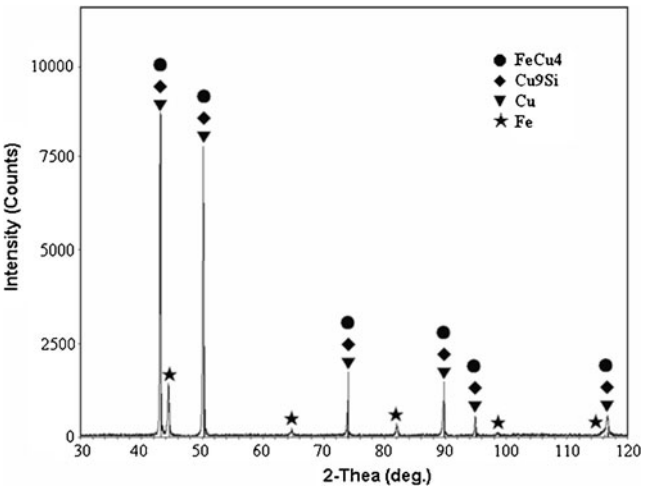

Fig. 11 XRD analysis on the bonding interface of the welding joint (diffraction angle 2θ is 10~90°)

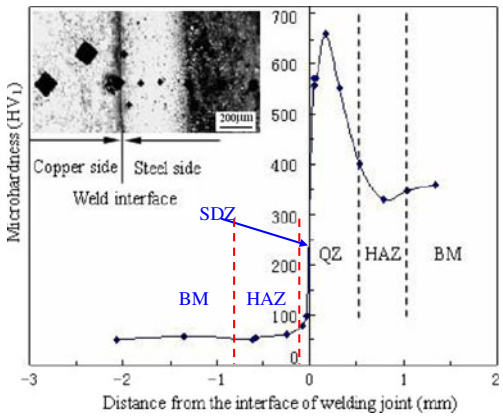

Fig. 12 Microhardness of the material in the IRFW joint

shows several factors, and the combined effects of heat transfer, stress, strain, and element diffusion associated with material dissimilarity should have played a role.

When Cu in T3 diffuses into the 35CrMnSi steel matrix (mainly concentrated in the interface region), Fe also diffuses into the T3 Cu side at the same time (so-called Fe element diffusion loss). After the exchange between Fe and Cu, the formation of new crystalline phases (such as $FeCu_4$ and Cu_9Si) do not change the microhardness of the QZ near the interface too much, which compare to the quenching martensite phase on the 35CrMnSi steel side.

In addition, because the content of the new crystalline phases are small, and the diffusion distance is very short, even though some new crystalline phase has a high microhardness value, the average microhardness should stay unchanged in QZ near the interface, which agrees with the rule of mixture. On the other hand, because the 35CrMnSi steel is of strong thermal-expansion ability, the middle of the QZ should experience a higher stress. Many thin lath martensites form should form in the 35CrMnSi steel side due to dynamic recrystallization, owing to deformation inhibition under a high friction welding temperature and a strong welding force.

With the increase of distance from weld interface to QZ, the diffusion content of Cu becomes less, the effect of Cu on the hardness of QZ decreases, and the thin lath martensites plays a main role to the hardness (see Fig. 7), the microhardness increases with the increasing of distance from interface to QZ. The microhardness value reduces in the HAZ, because the grains of the sorbite and ferrite in HAZ are rougher than that in BM, the micohardness value in HAZ is less than that in BM. So the microhardness value has a max peak value in the middle of QZ.

In one word, the microhardness of QZ is higher than that of BM, and the hardness of BM is higher than that of HAZ. The change of microhardness is a clear evidence on the combined influences of the microstructure, element diffusion and super-plastic deformation in T3/35CrMoSi dissimilar metal IRFW.

3.6 Interface bonding strength

Shear strength tests were conducted to evaluate the interface bonding because tensile strength is proportional to the shear strength. A standard shear testing method is carried out for the shear strength evaluation. The thickness of sliced samples is 2 mm and the tests follow GB/T6396 (China standard) clad plate mechanical and technological test in China. The results of shear strength values are shown in Fig. 14.

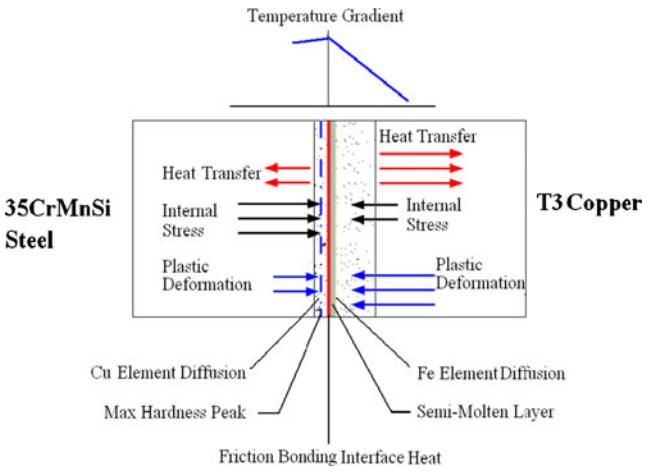

Fig. 13 Schematic of the factors affecting the interface of the dissimilar metal joint in IRFW

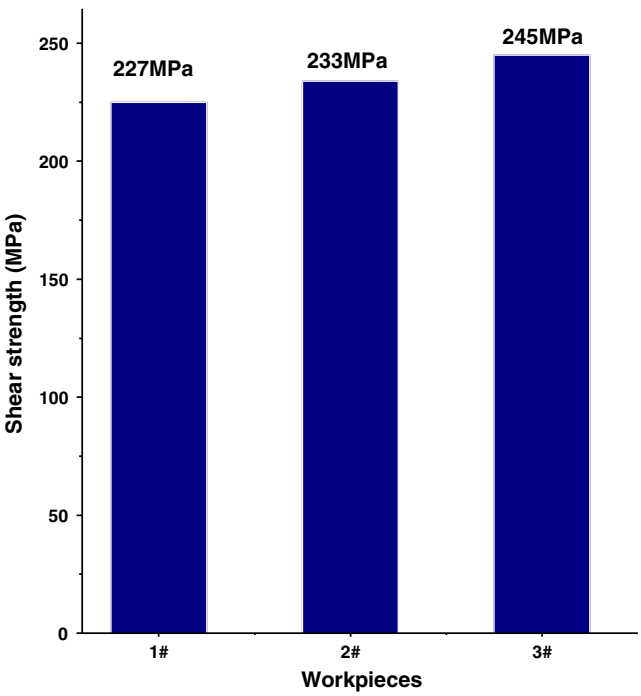

Fig. 14 Shear strength of the T3/35CrMnSi IRFW joint

The shear strength of all samples is higher than 200 MPa, and the maximum shear strength of the T3/35CrMnSi dissimilar metal IRFW joint is about 245 Mpa. These results indicate the success of IRFW, capable of meeting the requirements for its desired applications. Quality inspection indicates that, the rate of success of the joint production is higher than 98 %.

4 Conclusions

The work reported in this paper is a process to join T3 Cu and 35CrMnSi steel successfully by the IRFW technique. On the T3 Cu side, the SDZ is obvious and has a refined grain owing to the super-plastic deformation and dynamic recrystallization. Super-plastic deformation of the T3 Cu is close to a state of semi-melting because of friction heat. The formation mechanism of the fine grain layer on the SDZ of T3 Cu side is considered as the combined action of the semi-solid squeeze casting process method and super-plastic forge deformation method, based on the microstructure analyses of the T3/35CrMnSi dissimilar metal IRFW joints.

The bright white band forms on the 35CrMnSi steel side, which is defined as the QZ. The microstructure in the QZ is lath martensite, which is a different crystalline phase from that in the BM of 35CrMnSi (sorbite and ferrite). Lath martensite of the QZ is considered as a consequence of the heat treatment (quenching). There are three reasons for the formation of this zone: high welding temperature, dissimilar metal thermal-physical properties and short IRFW time. A new complete model is issued for affecting factors of the welding interface and is applied successfully to explain the interface characterization of T3 Cu/35CrMnSi dissimilar metal joints in IRFW.

Element diffusion phenomena are observed at both sides of the weld bonding interface, but the characterized elements (such as Si, Mn, and Cr element) of the 35CrMnSi steel are not detected on the T3 Cu side. Some new phases formed in the friction bonding interface. The $FeCu_4$ compound shows the landmark metallurgical bonding of T3/35CrMoSi dissimilar metals. A softening zone shows in the HAZ on the 35CrMnSi steel side. The maximum microhardness value lies in the middle of the QZ of the 35CrMnSi steel side, which is benefited from the quenching martensite microstructure, the new crystalline phase, the interface Fe-diffusion loss and a high stress in this layer. Shear strength testing indicates the successful joint of T3/35CrMnSi dissimilar metals joints by IRFW, which is capable of meeting the requirements for a desired application.

Acknowledgments The authors gratefully acknowledge support by the Natural Science Foundation of China (No. 51075413), the Fundamental Research Funds for the State Key Laboratory of Mechanical Transmission (SKLMT-ZZKT-2012MS08), Excellent Talents Project in Universities of Chongqing Municipal Education Commission and sharing fund of Chongqing university's large-scale equipment of P.R. China. The authors would like to thank Prof. Q Wang of Northwestern University, USA for helpful discussion.

References

1. Chen CM, Kovacevic R (2004) Joining of Al 6061 alloy to AISI 1018 steel by combined effects of fusion and solid state welding. Int J Mach Tools Manuf 44:1205–1214
2. Luo J, Li W, Sun Y, Wang X, Li Q (2009) Study on microstructure feature of joint interface of Cu–Al alloy thin-walled composite pipe. Mater Sci Technol 17:176–179
3. Magnabosco I, Ferro P, Bonollo F, Arnberg L (2006) An investigation of fusion zone microstructures in electron beam welding of copper–stainless steel. Mater Sci Eng A 424:163–173
4. Luo J, Sun Y, Liu D, Wu W, Xu X (2010) Characteristics of inertia radial friction welding joints of small size T3/35CrMnSi dissimilar metal materials. Chin J Nonferr Metals 20:1309–1315
5. Mai TA, Spowage AC (2004) Characterisation of dissimilar joints in laser welding of steel–kovar, copper–steel and copper–aluminium. Mater Sci Eng A 374:224–233
6. Luo J, Zhao G, Luo Q, Wang X, Xu X (2010) Element diffusion on interface of 35CrMnSi/T3 inertial radial friction weld. J Xi'an Jiaotong Univ 44:63–67
7. Sahin M (2009) Joining of stainless-steel and aluminum materials by friction welding. Int J Adv Manuf Technol 41:487–497
8. Jayabharath K, Ashfaq M, Venugopal P, Achar DRG (2007) Investigations on the continuous drive friction welding of sintered powder metallurgical (P/M) steel and wrought copper parts. Mater Sci Eng A 454–455:114–123
9. Sahin AZ, Yib BS, Ahmed M, Nickel J (1998) Analysis of the friction welding process in relation to the welding of copper and steel bars. J Mater Process Technol 82:127–136
10. Iordachescu M, Scutelnicu E (2008) An overview of welding in solid state. Annals "Dunarea de Jos" Univ Galati 12:31–38
11. Luo J, Lin Y, Luo Q, Wu Y (2004) New structure of automatic torch and new approach for controlling drop transfer in rotating spray welding arc. Sci Technol Weld Join 9:465–469
12. Luo J, Ye YH, Xu JJ, Luo JY, Wang XC, Liu KW (2009) A new mixed-integrated approach to control welded flashes forming process of damping tube-gland in continuous drive friction welding. Mater Design 30:353–358
13. Madhusudan Reddy G, Srinivasa Rao K (2009) Microstructure and mechanical properties of similar and dissimilar stainless steel electron beam and friction welds. Int J Adv Manuf Technol 45:875–888
14. Luo J, Luo Q, Lin YH, Xue J (2003) A new approach for fluid flow model in gas tungsten arc weld pool using longitudinal electromagnetic control. Weld J 82:202s–206s
15. Luo J, Wang XJ, Wang JX (2009) New technological methods and designs of stir head in resistance friction stir welding. Sci Technol Weld Join 14(5):650–654
16. Teker T (2012) Evaluation of the metallurgical and mechanical properties of friction-welded joints of dissimilar metal combinations AISI2205/Cu. Int J Adv Manuf Technol 56:1–8
17. Luo J, Montay G, Lu J (2005) An advanced residual stress determination for 3d cylinder structure using abaqus software. Mater Sci Forum 490–491:62–66
18. Moata R, Karadgea M, Preussa M, Brayb S, Martin R (2008) Phase transformations across high strength dissimilar steel inertia friction weld. J Mater Process Technol 204:48–58
19. Sahin M (2010) Joining of aluminum and copper materials with friction welding. Int J Adv Manuf Technol 49:527–534

20. Luo J (2001) A new measure technique and model for friction torque in continuous drive friction welding: engineering oriented voltage–current floating evaluation measurement method and exponential function model of friction torque. Sci Technol Weld Join 6:209–212
21. Spray JG (1988) Generation and crystallization of an amphibolites shear melt: an investigation using radial friction welding apparatus. Contrib Mineral Petrol 99:464–475
22. Du S, Wang Z, Cao Y, Wang J (2003) Influence of relative friction speed on the structure and properties of friction welding joint for dissimilar metals. Trans China Mech Eng Soc 14:1908–1910
23. Kore SD, Date PP, Kulkarni SV, Kumar S, Rani D, Kulkarni MR, Desai SV, Rajawat RK, Nagesh KV, Chakravarty DP (2011) Application of electromagnetic impact technique for welding copper-to-stainless steel sheets. Int J Adv Manuf Technol 54:949–955
24. Luo J, Zhao G, Wang X, Wu W, Xu X (2010) Effects of flywheel rotation speed on properties of 35CrMnSi/T3 inertial radial friction welding. J Chongqing Univ 33:24–28
25. Chen WW, Wang Q (2008) Thermomechanical analysis of elasto-plastic bodies in a sliding spherical contact and the effects of sliding speed, heat partition, and thermal softening. ASME J Tribol 130:1–10
26. Chen WW, Kim W, Wang Q (2009) Transient thermomechanical analysis of sliding electrical contact of elasto-plastic bodies, thermal softening and melting inception. ASME J Tribol 131:1–10
27. Xiaoling X, Wei W, Yuanze X (2005) Research of radial friction welding. Weld World 112:12–15
28. Nicholas ED (1983) Radial friction welding. Weld J 62:17–29
29. Xiaoling X, Yuanze X, Wei W (2008) Research on radial friction welding of 30 mm shell's band. J China Ordnance 4:69–71